Journal of Power Sources 284 (2015) 236–244

Contents lists available at ScienceDirect

Journal of Power Sources

journal homepage: www.elsevier.com/locate/jpowsour

Electrophoretic lithium iron phosphate/reduced graphene oxide composite for lithium ion battery cathode application

Yuan Huang [a, 1], Hao Liu [a, b, 1], Yi-Chun Lu [c], Yanglong Hou [d], Quan Li [a, *]

[a] Department of Physics, The Chinese University of Hong Kong, Shatin, New Territory, Hong Kong
[b] School of Science, China University of Geosciences (Beijing), Beijing, PR China
[c] Department of Mechanical and Automation Engineering, The Chinese University of Hong Kong, Shatin, New Territory, Hong Kong
[d] Department of Materials Science and Engineering, College of Engineering, Peking University, Beijing, PR China

HIGHLIGHTS

- A binder/additive free composite electrode was realized using electrophoresis.
- The high mass fraction of LFP reaches 91.5 wt%.
- Effective rGO network and intimate contact between rGO and LFP are formed.
- The composite electrode shows high capacity and excellent cyclability.
- This method can be applied to a variety of composited cathode or anode systems.

GRAPHICAL ABSTRACT

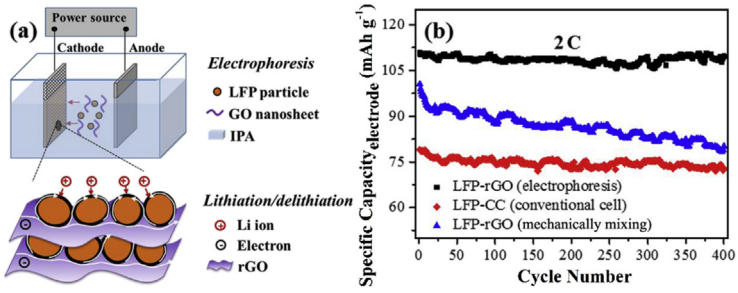

ARTICLE INFO

Article history:
Received 16 December 2014
Received in revised form
2 March 2015
Accepted 5 March 2015
Available online 6 March 2015

Keywords:
Electrophoresis
Graphene
Lithium iron phosphate
High mass fraction
Lithium ion battery

ABSTRACT

A binder/additive free composite electrode of lithium iron phosphate/reduced graphene oxide with ultrahigh lithium iron phosphate mass ratio (91.5 wt% of lithium iron phosphate) is demonstrated using electrophoresis. The quasi-spherical lithium iron phosphate particles are uniformly connected to and/or wrapped by three-dimensional networks of reduced graphene oxide nanosheets, with intimate contact formed between the two. Enhanced capacity is achieved in the electrophoretic composite cathode, when compared to either the conventional one or composite cathode formed by mechanically mixing lithium iron phosphate and reduced graphene oxide. The present methodology is simple and does not disturb the active material growth process. It can be generally applied to a variety of active material systems for both cathode and anode applications in lithium ion batteries.

1. Introduction

Lithium iron phosphate (LFP) is a most promising cathode material for lithium ion batteries (LIBs) due to its high theoretical capacity (170 mAh g^{-1}), flat voltage plateau, long cycle life, abundant material supply, and excellent safety [1–5]. A major problem of LFP is its low electronic conductivity, resulting in sacrificed capacity and low rate performance of the cathode [1–3].

Recently, introducing graphene to the active materials in order to form LFP/graphene (LFP/G) composite has been proposed as an effective means to improve the electronic conductivity of the

* Corresponding author.
E-mail address: liquan@phy.cuhk.edu.hk (Q. Li).
[1] These authors have equally contributed.

http://dx.doi.org/10.1016/j.jpowsour.2015.03.037
0378-7753/

cathode, and thus maximize the capacity and enhance the rate performance. There are two commonly employed methodologies for fabricating the LFP/G composite. One is hydrothermal/solvothermal growth of LFP nanoparticles from precursor on the pre-existing graphene [6]. The size of LFP synthesized by this method is usually small, which is another factor contributing to the improved electronic conductivity of the composite cathode, in addition to the effect brought by graphene introduction. Therefore, independently evaluating the contribution from graphene introduction remains challenging, as the LFP particles synthesized by different researchers are barely comparable, and they are much different from the commercially available ones. The other method is mechanically mixing of LFP and graphene [7,8]. Such a method can employ commercially available LFP particles, and the fabrication process is simple. Nevertheless, for both methods attempted, binders (and usually additional additives) must present in order to make a workable device. This is done at the expense of reduced active material content. In addition, an optimum content for graphene is always suggested to be necessary, usually ranging from 2 to 10% [7–9]. On the one hand, adequate amount of graphene is needed to form a 3D connecting network for effective charge transport in the cathode. On the other hand, too much graphene results in low packing density of the hybrid composite, and thus limiting the practical application. Moreover, additional additives (such as carbon black or super P with mass ratio ranging from 8% to 20%) are introduced in most case [6–10], and it suggests unsatisfactory device performance with graphene only [11]. Therefore, minimization of the graphene (and binders/other additives) and increase the mass ratio of the active material, while maintaining satisfactory cathode performance is highly desired.

Electrophoresis is an economical and versatile processing technique that has already been applied to the deposition of graphene or graphene/anode materials composite [12,13]. The technique has many merits, such as high deposition rate and throughput, good uniformity and controlled thickness of the obtained films, and simplicity of scaling up [14]. Seo et al. have fabricated a uniform graphene nanosheets/multiwalled carbon nanotubes composite film on Ni foil by using electrophoretic deposition and evaluated their electrochemical performance for LIBs anode applications [12]. Bae et al. prepared densely packed Sn/graphene nanocomposite by similar method and obtained binder-free Sn/graphene anode [13]. Nevertheless, little work is available for electrophoretic cathode materials employing graphene-based composite. Most recently, Sreelakshmi et al. showed the first work of electrophoretic $LiMn_2O_4$-graphene composite [15]. However, a thin composite film has been attempted and the highest ratio of $LiMn_2O_4$ only reaches ~74% (being comparable to that of the conventional cells or mechanically mixed ones), while the reason behind is not known.

In the present work, we have developed a fabrication method for LFP/G composite using electrophoresis that results in a binder/additive free composite cathode on fibrous substrate (carbon cloth) with extremely high LFP mass ratio. Comparing to the conventional LFP cell and mechanically mixed composite cathode (with similar composition as the electrophoretic one), we demonstrate considerably improved electrochemical performance of the electrophoretic LFP/G composite. The structure, composition and electrochemical properties of the electrophoretic composite cathode have been characterized. The key parameters during the composite cathode fabrication, including the specific ion (Mg^{2+} in the present case) concentration, processing temperature, and amount of graphene, have been systematically investigated and their individual roles have been elaborated.

2. Experimental

2.1. Electrophoresis of LFP/rGO composite on carbon cloth

The graphene oxide (GO) was prepared using the modified Hummers method [16]. The commercial LFP powders (Advanced Lithium Electrochemistry Co., Ltd., Taiwan) were employed as the active material. In a typical electrophoretic process, 25 mg LFP powder and 5 mg GO were separately dispersed in 5 mL isopropyl alcohol (IPA) by sonication for 3 h, and then mixed to form a uniform suspension. Additional 5 mg $Mg(NO_3)_2 \cdot 6H_2O$ was added to modify the surface of the GO sheets and LFP particles with positive charge. Two-electrode set-up, consisting a carbon cloth (8 mm × 8 mm) and a platinum foil electrode with a distance of 1 cm, was employed for the electrophoresis. A negative bias with magnitude of 90 V was applied to the carbon cloth substrate for depositing of LFP particles and GO nanosheets. Finally, the sample was reduced at 700 °C for 1 h under H_2 (volume 10%)/Ar atmosphere.

2.2. Structure and morphology characterization

The morphologies and elemental analyses were characterized by a field-emission scanning electron microscope (FESEM, Quanta 200, FEI). Transmission electron microscopy (TEM) measurements were also carried out with a Tecnai F20 (FEI) microscope operating at 200 kV. X-ray photoelectron spectroscopy (XPS, Thermo Fisher Scientific ESCALAB 250) with amonochromatic Al Ká radiation source was employed to investigate the elemental composition of the GO surface after reduction. The crystallinity and phases of the samples were examined by X-ray diffraction (XRD, SmartLab, Rigaku) with a Cu-Ka radiation source (d = 0.1541 nm). Raman analysis was performed using a Micro Raman spectrometer (RM-1000, Renishaw Co., Ltd.) with a 10 mW helium–neon laser at 514 nm. Thermal gravimetric analysis (TGA, Perkin–Elmer) was employed to quantify the amount of reduced graphene oxide (rGO) in the LFP/rGO composite.

2.3. Electrochemical characterization

The electrochemical properties of the LFP/rGO composite were characterized by using CR2032 coin-type cells with Li foil as a counter electrode. The liquid electrolyte was 1.0 M $LiPF_6$ in the mixture of 1:1 (by volume) ethylene carbonate and diethyl carbonate (Novolyte Co.). No binder or conducting carbon was additionally used. As a comparison, a conventional cell (79 wt% LFP powder, 10 wt% acetylene black, and 10 wt% polyvinylidene fluoride (PVDF)) with adding a small amount of $Mg(NO_3)_2 \cdot 6H_2O$ (around ~1 wt%) on carbon cloth was prepared. In order to better understand the role of rGO in the LFP/rGO composite, another LFP/rGO composite was obtained by mechanically mixing of LFP particles and GO nanosheets with a small amount of $Mg(NO_3)_2 \cdot 6H_2O$ (around ~1 wt%), before reduced at 700 °C for 1 h under H_2 (volume 10%)/Ar atmosphere. The final electrode consisted of 94 wt% LFP/rGO composite (the mass ratio between LFP and rGO was kept same as the electrophoretic samples), 1 wt% Mg^{2+}, and 5 wt% PVDF binder. Cyclic voltammertry (CV) was conducted at a scanning rate of 0.1 mV s^{-1} between 2.5 and 4.2 V *vs.* Li^+/Li (CHI660, Shanghai CH Instrument Co., Ltd.). Galvanostatic charging/discharging cycles were tested between 2.5 and 4.2 V *vs.* Li^+/Li at different rates on a multichannel battery test system (CT2001A, Wuhan Kingnuo Electronic Co., Ltd.). The electrochemical impedance spectroscopy (EIS) of the batteries was performed in the frequency range from 100 kHz to 0.3 Hz under an alternating current (AC) stimulus with a 5 mV amplitude (CHI 660C, Shanghai CH Instrument Co., Ltd.). The

impedance data were fitted using the ZView program.

3. Results and discussions

3.1. General characterizations of the electrophoretic samples

Fig. 1(a) illustrates the deposition process of LFP/GO composite on carbon cloth using electrophoresis. Details on the fabrication procedures can be found in the Experimental section. After deposition, the LFP/GO composite was annealed under H_2/Ar atmosphere to obtain the LFP/rGO composite. The general morphology and structure of all electrophoretic samples are similar, and here we show the results of a representative one, i.e., the electrophoretic LFP/rGO composite with 7.5 wt% rGO annealed at 700 °C. The amount of Mg in this sample is ~1 wt%. We name such a sample as LFP-rGO (E 7.5%)-700.

The SEM image shown in Fig. 1(b) discloses the quasi-spherical LFP particles uniformly connected to/wrapped by rGO nanosheets. The sizes of the LFP particles (diameter) range from ~100 to ~800 nm, with an average at ~350 nm (Fig. S1, Supporting Information). The EDX (Fig. 1(c)) taken from the same sample shows that it is mainly composed of C, O, P, and Fe with trace amount of Mg (added during electrophoresis, and its role will be discussed in later sections). The atomic ratio of Fe, P, and O elements is ~1:1:4 (Table S1, Supporting Information), being consistent with that of the stoichiometry $LiFePO_4$.

The crystallinity of LFP after the composite formation is found to be similar to that of the commercial LFP. XRD results of both samples are shown in Fig. 1(d). All Bragg peaks can be indexed to the orthorhombic LFP phase. Obvious reflection from rGO is not observed due to its very low content in the composite. The Raman spectrum in Fig. 1(e) discloses the degree of graphitization of carbon in the LFP/rGO composite [8]. The D band at 1351 cm^{-1} is attributed to defects and disordered portions of carbon (sp^3), whereas the G band at 1598 cm^{-1} is indicative of ordered graphitic crystallites of carbon (sp^2) [17]. The intensity ratio of D band to G

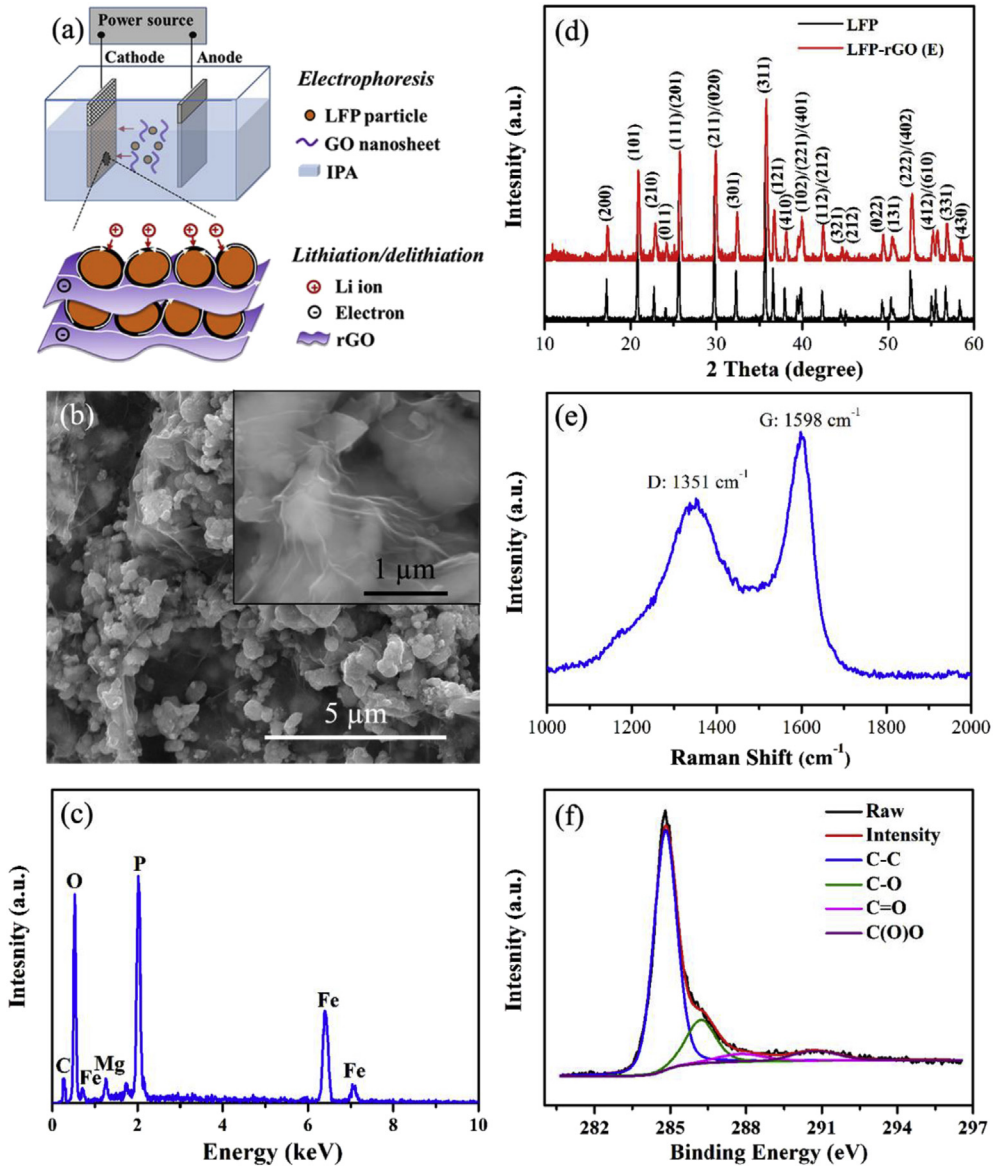

Fig. 1. (a) Schematic of the electrophoresis process employed to prepare LFP/GO composite on carbon cloth. (b) SEM image of the annealed LFP-rGO (E 7.5%)-700 sample on carbon cloth. The inset is the SEM image of same sample taken at higher magnification. (c) EDX spectrum taken from the same sample. (d) XRD spectra of the commercial LFP powder and LFP-rGO (E 7.5%)-700 composite formed on carbon cloth. (e) Raman spectrum taken from the LFP-rGO (E 7.5%)-700 composite. (f) XPS spectra (C 1s) of the same sample.

band (I_D/I_G) is related to the extent of π-conjugation and concentration of defects. A relatively low D band to G band ratio (I_D/I_G ~ 0.77) measured from the present sample indicates the dominant presence of sp^2-coordinated carbon in the LFP/rGO composite. We then examine the extent of GO reduction to rGO (700 °C annealing) using XPS. The C1*s* peak of the rGO (Fig. 1(f)) can be deconvoluted into four different peaks centered at 284.8 eV (corresponding to sp^2 C), 286.2 eV (C–O), 287.8 eV (C═O), and 290.7 eV (C(O)O) [18]. Although some oxygen-containing functional groups remain, the low intensities of the C–O, C═O, and C(O)O peaks indicate efficient reduction of GO in the composite after 700 °C annealing under H_2/Ar atmosphere. This is consistent with literature results of GO reduction [18].

More detailed structural characterizations of the LFP-rGO (E 7.5%)-700 sample have been carried out using TEM. Fig. 2(a) shows that LFP nanoparticles anchor onto the rGO sheets. An amorphous carbon layer (~3–4 nm) presents on the surface of the LFP nanoparticle (Fig. 2(b)). This carbon coating is part of the commercial LFP powder (Fig. S2, Supporting Information). EDX elemental mapping gives the spatial distribution of the compositional elements (Fig. 2(c)–(i)). It reveals the correlation between the LFP nanoparticles and the rGO. In addition, the Mg elemental map suggests that Mg covers most of the rGO surface (Fig. 2(h)) in a rather uniform manner.

3.2. Comparison among electrophoretic sample, conventional cell, and mechanically mixed sample

The electrochemical properties of the electrophoretic LFP-rGO (E 7.5%)-700 electrode (this sample has 7.5 wt% rGO, 91.5 wt% LFP, and 1 wt% Mg^{2+}, and was denoted as LFP-rGO (E) for short in the following) have been compared to those of the conventional LFP electrode (LFP-CC, 79 wt% LFP powder, 1 wt% Mg^{2+}, 10 wt% acetylene black, and 10 wt% PVDF binder) and the LFP/rGO composite

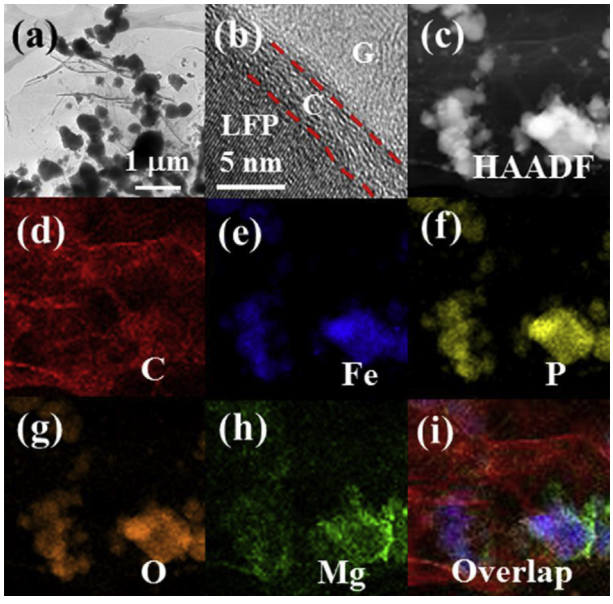

Fig. 2. (a) Low magnification TEM image taken from the LFP-rGO (E 7.5%)-700 composite sample. (b) High resolution TEM image taken from the surface regions of LFP particle, disclosing the rGO surface layer and the amorphous carbon wrapping LFP. (c) High angle annular dark field (HAADF) image taken from part of this composite sample. (d)–(i) EDX elemental maps taken from the same region shown in Fig. 2(c). (d) C; (e) Fe; (f) P; (g) O; and (h) Mg maps. (i) Color map of C, Fe, and Mg, showing the spatial correlation among rGO, LFP, and Mg. (For interpretation of the references to colour in this figure legend, the reader is referred to the web version of this article.)

electrode made by mechanically mixing the two (LFP-rGO (M), with the same LFP/rGO ratio as the electrophoretic sample, 1 wt% Mg^{2+}, and additional 5 wt% PVDF). To make the three samples more comparable, the same annealing process was applied to the respective as-prepared samples. More details of the electrodes preparation can be found in the Experimental section. The morphology of LFP-rGO (M) sample is presented in Fig. S3 (Supporting Information).

Fig. 3(a) shows cyclic voltammogram of the LFP-rGO (E), LFP-CC, and LFP-rGO (M) samples at a scan rate of 0.1 mV s^{-1} in voltage range of 2.5–4.2 V *vs.* Li^+/Li. The three samples show typical oxidation/reduction peaks during the anodic/cathodic scan, corresponding to the reversible redox reaction between Fe^{2+}/Fe^{3+} in LFP particles. Nevertheless, their shape, the potential intervals between the two redox peaks, and current density of peak are different. For the LFP-CC and LFP-rGO (M) samples, wide and low peaks with potential intervals of ~0.260 and ~0.241 V have been respectively observed. As a comparison, the LFP-rGO (E) sample shows sharp and high symmetric peaks with the smallest potential interval of ~0.220 V, indicating the low polarization and high reversibility of this sample. One may notice the small capacitive behavior of the rGO-based samples. This is due to the fact that restacking of the rGO sheets under the van der Waals forces would reduce its effective surface area [19].

Fig. 3(b) shows the first charging and discharging profiles of the three samples at low rate of 0.1 C. The average plateau is around 3.44 V *vs.* Li^+/Li for all samples, corresponding to the Fe^{2+}/Fe^{3+} redox reaction. The polarization between the charging and discharging plateuas for the LFP-rGO (E), LFP-CC, and LFP-rGO (M) samples are ~40.3, ~55.8, and 54.9 mV. The smaller polarization of the LFP-rGO (E) sample than the other two indicates the lowest internal resistance of such a sample. This is consistent with the cyclic voltammogram data (Fig. 3(a)). As a result, the LFP-rGO (E) sample also delivers highest discharging capacity of ~163.7 mAh g^{-1} (normalized over the total mass of the whole electrode) at 0.1 C rate, while the LFP-CC and LFP-rGO (M) samples exhibit discharging capacity of ~106.3 and 132.8 mAh g^{-1} at same rate (Fig. 3(b)).

Fig. 3(c) shows comparison of the rate performance of the three samples (the capacity is normalized over the total mass of the whole electrode). Again, the LFP-rGO (E) sample exhibits the best rate capability among the three samples. For example, the LFP-rGO (E) sample can deliver discharging capacity of 163.7 mAh g^{-1} at low rate of 0.1 C. When the discharging rate increases to higher values such as 5 C and 10 C, the discharging capacities are maintained at ~98.5 and ~82.4 mAh g^{-1}, respectively. As a comparison, the LFP-rGO (M) sample exhibits much lower discharging capacity, that is, ~85.1 mAh g^{-1} at 5 C rate and ~73.4 mAh g^{-1} at 10 C rate. The LFP-CC sample exhibits the worst rate performance.

The cycling performance of the LFP-rGO (E) sample is also improved especially at high rates when compared to other two samples (Fig. 3(d)). At high rate of 2 C, little decay in the discharge capacity (over the mass of the total electrode) of the LFP-rGO (E) sample is observed-109.7 mAh g^{-1} (98.92% of 110.9 mAh g^{-1}) is maintained after 400 cycles, indicating the excellent cycling stability of the LFP-rGO (E) sample. As a comparison, the discharging capacity of the LFP-rGO (M) sample decreases from the initial value of ~100.5 mAh g^{-1} to ~80.1 mAh g^{-1} at rate of 2 C after 400 cycles.

The fact that the electrophoretic LFP/rGO composite cathode shows improved electrochemical performance compared to the mechanically mixed one suggests that electrophoresis is a superior fabrication method than mechanically mixing. In fact, electrophoresis is known to deposit densely packed active materials due to the influence of an electric field. It is capable of producing uniform deposits with an intimate interface between active materials (LFP

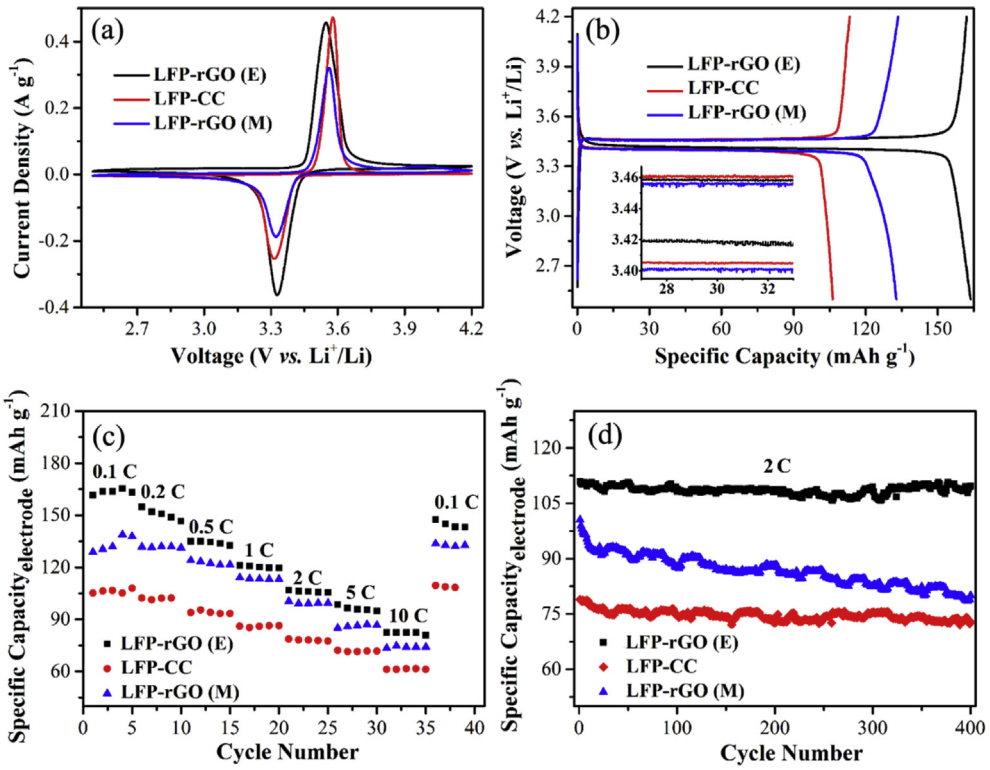

Fig. 3. (a) Cyclic voltammogram of the electrophoretic (LFP-rGO (E)), mechanically mixed (LFP-rGO (M), with the same LFP/rGO ratio as the electrophoretic sample), and conventional (LFP-CC) samples at a scan rate of 0.1 mV s^{-1} in 2.5–4.2 V *vs.* Li^+/Li. (b) Comparison of the first charging and discharging profiles of the three samples at a rate of 0.1 C. (c) Specific capacities (normalized over the total electrode mass) of the three samples at various rates. (d) Cycling stability of the three samples cycled at a rate of 2 C.

in the present case) and graphene (rGO in the present case). The electrophoretic method has additional advantage of generating samples free of binders and other additives. All these characteristics contribute to the improved capacity as well as enhanced rate performance and cyclability of the electrophoretic samples.

3.3. Structure and morphology stability of the electrophoretic LFP/rGO composite cathode after the cycling test

In order to examine the structure stability of the LFP-rGO (E 7.5%)-700 sample, the morphological changes were characterized at lithiated state after the cycling test. Before the disassembling, the cell was held at 2.5 V *vs.* Li^+/Li for 12 h. One can observe that the LFP/rGO composite structure after cycling remains nearly uncharged (Fig. S4(a), Supporting Information) as compared to the morphology of the pristine LFP/rGO composite (Fig. 1(b)), except that the average size of LFP particles increases from ~350 nm to ~370 nm (Fig. S5, Supporting Information), likely contributed by the surface-passivating layer or SEI layer on the LFP surface. TEM image and EDX element maps (Fig. S4(b)–(i), Supporting Information) further confirm the morphological/structural similarity in the LFP/rGO composite samples before and after cycling. The experimental results suggest good structural stability of the electrophoretic LFP/rGO composite electrode.

3.4. Effect of different fabrication parameters on the electrochemical performance of the electrophoretic LFP/rGO composite cathode

3.4.1. Mg^{2+} amount

Mg^{2+} is suggested to have multiple roles in the electrophoresis of the LFP/rGO cathode. First of all, the presence of Mg^{2+} changes the surface charge of GO and LFP. In fact, we have found that electrophoresis of LFP and GO is possible on the cathode in the absence of Mg^{2+}, but the deposition rate is very low, so that the total amount of LFP and GO that can be deposited onto the electrode is very limited. When Mg^{2+} is introduced during the electrophoresis, LFP and GO are found to be deposited onto the anode, and a much denser and better-adhered layer of LFP/GO composite can be formed. As a matter of fact, Mg^{2+} is known to improve the adhesion of GO onto the current collector during electrophoresis of GO, likely due to the formation of metal hydroxide of Mg^{2+} at the current collector surface [14,20].

The effect of the amount of Mg^{2+} added is investigated by adjusting the mass ratio of Mg^{2+} (1%, 5%, >10%) in the electrophoretic LFP-rGO (E 7.5%)-700 composite sample. If the amount of Mg^{2+} is larger than 10 wt%, a mass of floccules are observed on the skeleton of carbon cloth after the electrophoretic process (Fig. S6, Supporting Information) but the amount of LFP and GO deposited onto the electrode is very limited. This is a result of the hydrolysis of Mg^{2+} that leads to the formation of large amount of $Mg(OH)_2$ [20] and makes further deposition of active materials difficult. At lower Mg^{2+} amount, e.g. 1 wt% and 5 wt%, a good layer of LFP/GO can be formed on the carbon cloth. Fig. 4(a) shows the cyclic voltammogram of the LFP-rGO (E 7.5%)-700 with small amount of Mg^{2+} (1 wt %, 5 wt%) at scan rate of 0.1 mV s^{-1} in voltage range of 2.5–4.2 V *vs.* Li^+/Li. For the LFP-rGO (E 7.5%)-700 sample with 1 wt% Mg^{2+}, sharp and high peaks with potential interval of ~0.220 V have been observed. As a comparison, the LFP-rGO (E 7.5%)-700 sample with 5 wt% Mg^{2+} shows wide and low symmetric peaks with the larger potential interval of ~0.258 V, indicating the high polarization and low reversibility of this sample. In addition, the LFP-rGO (E 7.5%)-700 sample with 1 wt% Mg^{2+}, delivers higher discharging capacity of ~174.7 mAh g^{-1} (normalized over the mass of the commercial

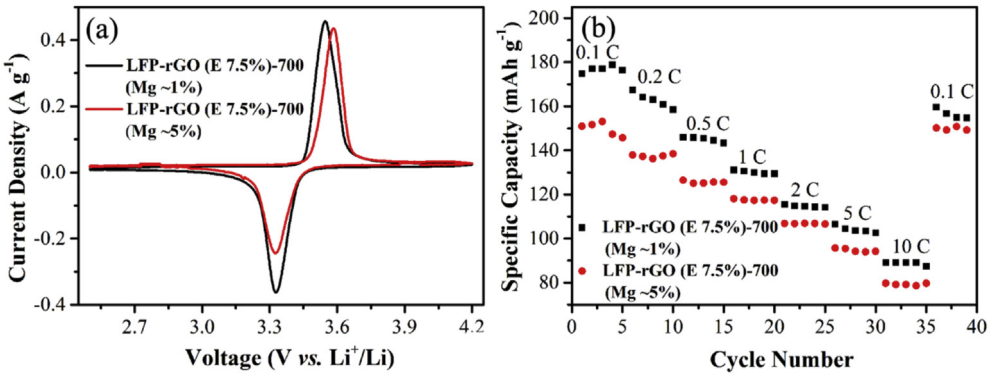

Fig. 4. (a) Cyclic voltammogram of the LFP-rGO (E 7.5%)-700 samples with different amount of Mg^{2+} at a scan rate of 0.1 mV s^{-1} in 2.5–4.2 V *vs.* Li^+/Li. (b) Comparison of the rate performance of the LFP-rGO (E 7.5%)-700 with different amount of Mg^{2+}.

LFP powder) at 0.1 C rate, while the LFP-rGO (E 7.5%)-700 sample with 5 wt% Mg^{2+} exhibits discharging capacity of ~150.9 mAh g^{-1} at same rate (Fig. 4(b)). When the discharging rate increases to higher values such as 5 C and 10 C, for the LFP-rGO (E 7.5%)-700 sample with 1 wt% Mg^{2+}, the discharging capacities are maintained at ~106.5 and ~89.1 mAh g^{-1}, respectively. As a comparison, the LFP-rGO (E 7.5%)-700 sample with 5 wt% Mg^{2+}, exhibits lower discharging capacity, that is, ~95.7 mAh g^{-1} at 5 C rate and ~79.7 mAh g^{-1} at 10 C rate. The poorer electrochemical performance of the LFP-rGO (E 7.5%)-700 sample with 5 wt% Mg^{2+} has been attributed to the over hydrolysis of Mg^{2+}. The more Mg^{2+} introduced into the suspension during electrophoretic process, the more $Mg(OH)_2$ formed, leading to reduced electronic conductivity of composite due to the poor conductivity of $Mg(OH)_2$. A proper Mg^{2+} amount (~1 wt%) is needed to maintain both effective deposition of LFP/GO on the substrate and satisfactory electrochemical performance of the resulted LFP/rGO composite electrode.

3.4.2. Post annealing temperature

LFP-GO (E 7.5%) composite sample with 1 wt% Mg^{2+} was further annealed at different temperatures of 450, 550, and 700 °C, under H_2/Ar atmosphere. The corresponding samples are referred as LFP-rGO (E 7.5%)-450, LFP-rGO (E 7.5%)-550, and LFP-rGO (E 7.5%)-700. It is worth noting the potential interval between the two redox peaks decrease with the annealing temperature increases, as shown in Fig. 5(a). The potential intervals of these three samples are ~0.283, ~0.262, and ~0.220 eV Fig. 5(b) shows comparison of the rate performance of the three samples. It is obvious that the LFP-rGO (E 7.5%)-700 sample exhibits the best rate capability among these samples. For example, at high rate of 10 C, LFP-rGO (E 7.5%)-700 sample can deliver discharging capacity of ~89.1 mAh g^{-1}. As a comparison, the LFP-rGO (E 7.5%)-550 sample exhibits lower discharging capacity, that is, ~71.2 mAh g^{-1} at 10 C. LFP-rGO (E 7.5%)-450 sample exhibits the worst rate performance. It has been reported electrical conductivity of rGO is closely related to the annealing temperature. Concomitant increase of the rGO conductivity was observed with an increase in the heating temperatures by Wang et al. [21]. With the increase of the annealing temperature, the improved conductivity is consistent with the declined potential interval between the two redox peaks, suggesting lower polarization of the electrodes.

3.4.3. rGO amount—minimizing the rGO content

In the electrophoretic LFP/rGO composite sample, we have attempted to adjust the mass ratio of rGO from ~5.3 wt% to ~11.8 wt %. The amount of rGO presented in the composite is evaluated using TGA (Fig. S7, Supporting Information). The corresponding samples are referred as LFP-rGO (E 5.3%)-700, LFP-rGO (E 7.5%)-700, and LFP-rGO (E 11.8%)-700. Fig. 6(a) shows cyclic voltammogram of the electrophoretic LFP/rGO composite samples with 5.3 wt%, 7.5 wt%, and 11.8 wt% rGO at scan rate of 0.1 mV s^{-1} in voltage range of 2.5–4.2 V *vs.* Li^+/Li. Among the three samples, the LFP-rGO (E 7.5%)-700 sample shows sharpest and highest symmetric peaks with the smallest potential interval of ~0.220 V, indicating the lowest polarization and highest reversibility of this sample. For LFP-rGO (E 5.3%)-700 and LFP-rGO (E 11.8%)-700 samples, wide and low peaks with potential intervals of ~0.267 and ~0.241 V have been respectively observed.

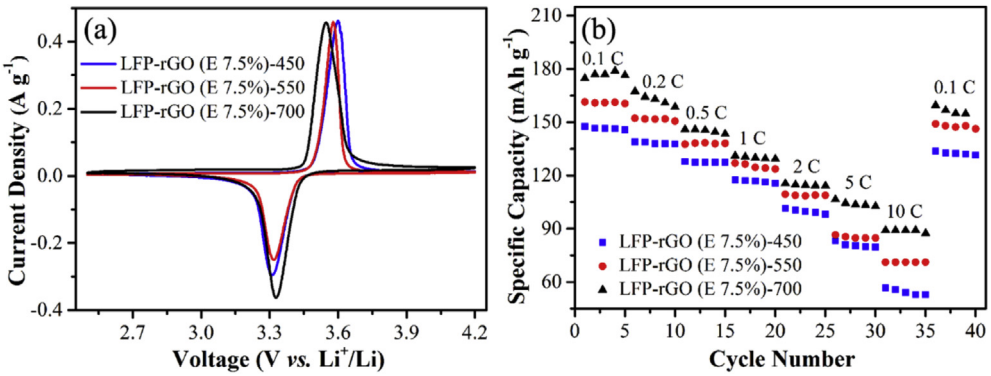

Fig. 5. (a) Cyclic voltammogram of the LFP-rGO (E 7.5%) annealed at different temperatures at scan rate of 0.1 mV s^{-1} in 2.5–4.2 V *vs.* Li^+/Li. (b) Comparison of the rate performance of the LFP-rGO (E 7.5%) annealed at different temperatures. The Mg^{2+} was at ~1 wt% for all three samples in this series.

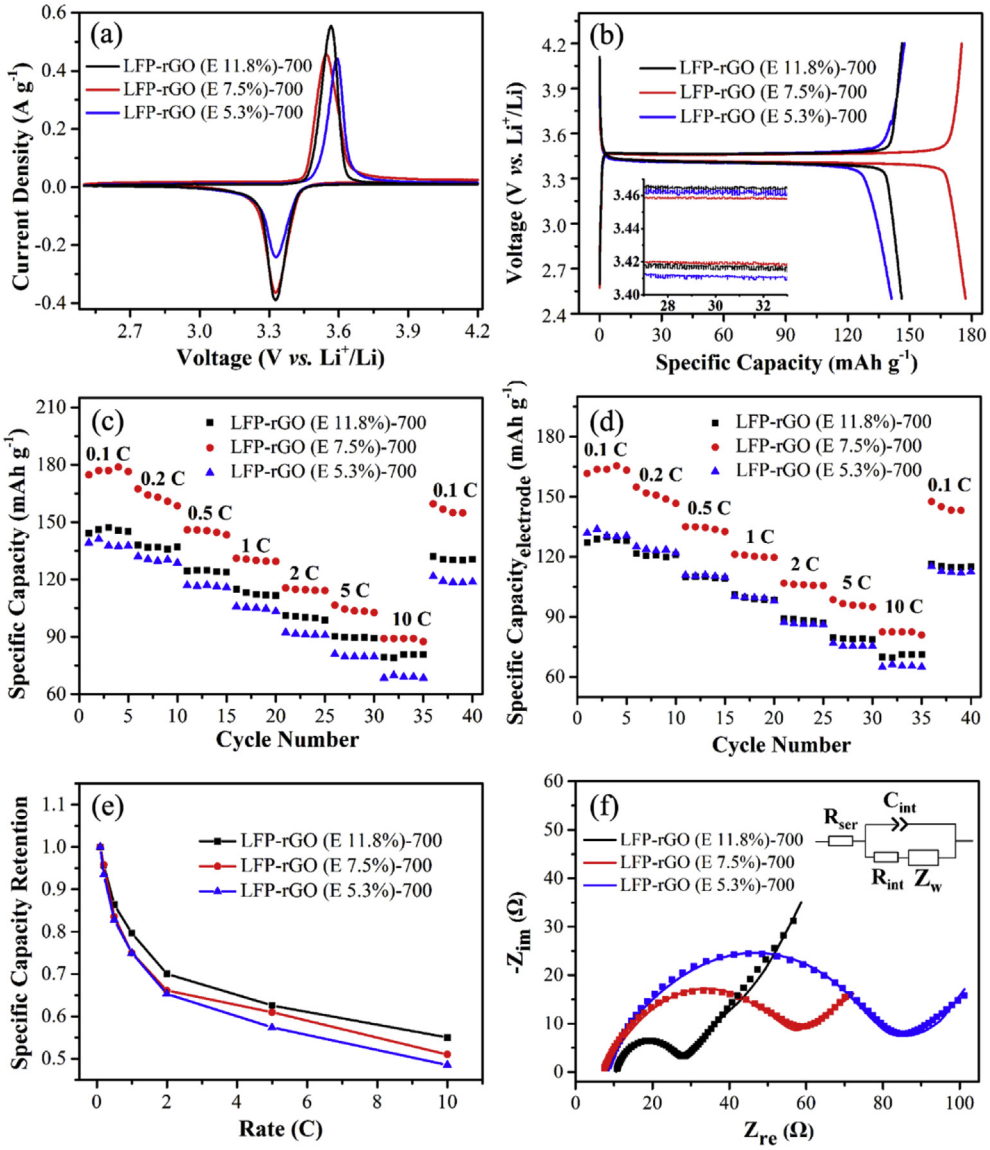

Fig. 6. (a) Cyclic voltammogram of the LFP-rGO (E 11.8%)-700, LFP-rGO (E 7.5%)-700, and LFP-rGO (E 5.3%)-700 samples at a scan rate of 0.1 mV s^{-1} in 2.5–4.2 V *vs.* Li^+/Li. (b) Comparison of the first charging and discharging profiles of the three samples at a rate of 0.1 C. (c) Specific capacities (normalized over the total mass of LFP) of the samples at various rates. (d) Specific capacities (normalized over the total mass of the electrode) of the samples at various rates. (e) Comparison of the specific capacity retention of the three samples. (f) Nyquist plots of the three samples after discharging to ~4.2 V *vs.* Li^+/Li.

Fig. 6(b) shows the first charging and discharging profiles of the three samples at low rate of 0.1 C. The average plateau is around 3.44 V *vs.* Li^+/Li for all samples, corresponding to the Fe^{2+}/Fe^{3+} redox reaction. The polarization between the charging and discharging plateuas for the LFP-rGO (E 5.3%)-700, LFP-rGO (E 7.5%)-700, and LFP-rGO (E 11.8%)-700 samples are ~51.4, ~40.3, and ~47.5 mV. The smaller polarization of LFP-rGO (E 7.5%)-700 sample than the other two indicates that this sample has lowest internal resistance, which is consistent with the cyclic voltammogram data (Fig. 6(a)).

Fig. 6(c) and (d) show comparison of the rate performance of the three samples. The specific capacity in Fig. 6(c) and (d) are normalized over the mass of LFP (specific capacity) and the mass of the whole electrode (specific $capacity_{electrode}$), respectively. It is obvious that the LFP-rGO (E 7.5%)-700 sample exhibits the highest specific capacity (or specific $capacity_{electrode}$) among these samples. For example, the LFP-rGO (E 7.5%)-700 sample can deliver discharging capacity of ~174.7 mAh g^{-1} at low rate of 0.1 C. It should be noted that the discharging capacity of the LFP-rGO (E 7.5%)-700 sample is slightly higher than the theoretical capacity of LFP (170 mAh g^{-1}). It is known that rGO can deliver 64 mAh g^{-1} at low charging/discharging rate [22]. Considering the weight percentage of rGO in the LFP-rGO (E 7.5%)-700 composite, the extra capacity (~4.7 mAh g^{-1}) at low rate of 0.1 C is probably contributed by the rGO nanosheets. When the discharging rate increases to higher values such as 5 C and 10 C, the discharging capacities are maintained at ~106.5 and ~89.1 mAh g^{-1}, respectively. As a comparison, the LFP-rGO (E 11.8%)-700 sample exhibits lower discharging capacity, that is, ~90.2 mAh g^{-1} at 5 C rate and ~79.3 mAh g^{-1} at 10 C rate. LFP-rGO (E 5.3%)-700 sample exhibits the lowest capacity. If the specific capacity is normalized over on the total mass of the whole electrode material (including both rGO, Mg, and LFP), the specific $capacity_{electrode}$ of the LFP-rGO (E 11.8%)-700 sample is close to that of the LFP-rGO (E 5.3%)-700 sample at various rate, while LFP-rGO (E 7.5%)-700 sample remains the best, as shown in Fig. 6(d). Unlike the specific capacity, the capacity retention would

improve when more rGO is incorporated, and the best capacity retention is achieved in the LFP-rGO (E 11.8%)-700 sample, as shown in Fig. 6(e).

These results disclose the role of rGO in the composite electrode: On the one hand, one needs to have adequate amount of rGO forming connecting networks for hosting the active material, so that all LFP grains are accessible during the cycling. This helps to increase the specific capacity of the composite cathode. However, rGO also contributes to the measured capacity and its specific capacity is much smaller than that of the LFP. Therefore, higher amount of rGO means lower LFP mass ratio in the composite electrode, providing an explanation for the lower specific capacity of LFP-rGO (E 11.8%)-700 sample as compared to the LFP-rGO (E 7.5%)-700 sample, especially when the capacity is normalized over the total electrode mass. On the other hand, larger amount of rGO contributes to the formation of a more complete conductive network, and such contribution would be "amplified" when the cell performs at higher rates. This explains the improved capacity retention of LFP-rGO (E 11.8%)-700 sample (as shown in Fig. 6(e)).

To obtain better understanding on the difference among the three samples, the EIS measurements were carried out after discharging the samples to ~4.2 V *vs.* Li^+/Li. The corresponding Nyquist plots are shown in Fig. 6(f). A typical Nyquist plot of LIBs consists of these characteristic features: the depressed semicircle at the high-to-medium frequency range, followed by an inclined line at the low frequency region. The intercept of the real axis at high frequency is dominated by series ohmic resistance, which is contributed by external cell connections and ionic conduction through the electrolyte and separator. The semicircle at high-to-medium frequency region corresponds to the interfacial resistance resulting from charge transfer resistance on the electrode interface and the presence of a passivating SEI layer. The inclined line at 45° in low frequency region represents the diffusion of Li^+ in the solid-state electrode, which is also named as Warburg impedance [23]. When the frequency further decreases, it shows a semi-infinite diffusion element due to the presence of the current collector interface [24]. The single depressed semicircle in Fig. 6(f) indicates the high-frequency semicircle and medium-frequency semicircle overlap with each other. Therefore, an appropriate equivalent circuit model (inset of Fig. 6(f)) is established to generate the best fit for the Nyquist curves. The fitting parameters (e.g., R_{ohm} and R_{int}) are shown in Table S2 in the Supporting Information. The series resistances of the three samples are similar (in the range of several Ohms). Nevertheless, the interfacial resistance R_{int} at the electrode/electrolyte interface is 16.33 Ω for LFP-rGO (E 11.8%)-700 sample, being much smaller than those of the other two samples (Fig. 6(f)). The LFP-rGO (E 5.3%)-700 sample shows the highest value of R_{int} among the three. The smallest interfacial resistance in the LFP-rGO (E 11.8%)-700 sample is consistent with its best capacity retention among the three samples.

In order to examine the impact of rGO on the Li^+ transport properties, the effective Li^+ diffusion coefficient was estimated from the EIS data based on the equation $D_{Li} = r^2/W_{-T}$, in which D_{Li} is the effective Li^+ diffusion coefficient, r is the radius of LFP particles, W_{-T} is the fitting parameter of Warburg element [23,24]. Here, r is represented by the mean radius of LFP particles (~175 nm obtained from size statistic in Fig. S1). The estimated values of the D_{Li} are ~1.62×10^{-11}, ~2.04×10^{-11}, and ~3.00×10^{-11} $cm^2\ s^{-1}$, corresponding to the LFP-rGO (E 5.3%)-700, LFP-rGO (E 7.5%)-700, and LFP-rGO (E 11.8%)-700 samples (Fig. 6(f) and Table S2 in Supporting Information). It indicates that different amount of rGO incorporation does not significantly affect the Li^+ diffusion in these samples.

4. Conclusions

We demonstrate that electrophoresis can effectively couple the LFP and rGO to form a binder/additive free composite electrode with achieving high LFP mass ratio. By optimizing the processing parameters, LFP/rGO composite sample with 7.5 wt% rGO, 1 wt% Mg^{2+}, and being annealed at 700 °C exhibits the highest capacity. The introduction of Mg^{2+} modifies the surface charge of both LFP and GO, and improves the adhesion of the electrophoretic LFP/GO on the substrate. However, the hydrolysis of excessive Mg^{2+} leads to the formation of too much $Mg(OH)_2$, which not only affects the LFP/GO deposition but also deteriorates the composite electrode performance. Higher annealing temperature is found to more effectively reduce GO, leading to increased electronic conductivity of the composite sample, and thus improve the electrochemical performance. Adequate amount of rGO is necessary for obtaining decent electronic conductivity of the composite electrode, but too much rGO would reduce the overall specific capacity of the electrode, due to the low capacity of rGO. When compared to conventional battery and LFP/rGO composite sample made by mechanically mixing of LFP and rGO, the electrophoretic LFP/rGO composite cathode shows largely enhanced capacity and excellent cycling stability, suggesting the effective rGO network realized and intimate contact formed between rGO and LFP by electrophoresis. Comparing to LFP/rGO composite formed by other growth method (e.g. LFP/G co-growth using LFP precursors), the present methodology is simple and does not disturb the active material growth process. It can be generally applied to a variety of active material systems for both cathode and anode applications in LIBs.

Acknowledgments

This work is supported by General Research Funding of the National Natural Science Foundation of China/Research Grants Council Joint Research Scheme under project No. N_CUHK448/13.

Appendix A. Supplementary data

Supplementary data related to this article can be found at http://dx.doi.org/10.1016/j.jpowsour.2015.03.037.

References

[1] L.X. Yuan, Z.H. Wang, W.X. Zhang, X.L. Hu, J.T. Chen, Y.H. Huang, J.B. Goodenough, Energy Environ. Sci. 4 (2011) 269–284.
[2] W.J. Zhang, J. Power Sources 196 (2011) 2962–2970.
[3] J. Wang, X. Sun, Energy Environ. Sci. 5 (2012) 5163–5185.
[4] P. Bai, M.Z. Bazant, Nat. Commun. 5 (2014) 3585.
[5] Y. Zhao, L. Peng, B. Liu, G. Yu, Nano Lett. 14 (2014) 2849–2853.
[6] C. Su, X. Bu, L. Xu, J. Liu, C. Zhang, Electrochim. Acta 64 (2012) 190–195.
[7] L.H. Hu, F.Y. Wu, C.T. Lin, A.N. Khlobystov, L.J. Li, Nat. Commun. 4 (2013) 1687.
[8] X. Zhou, F. Wang, Y. Zhu, Z. Liu, J. Mater. Chem. 21 (2011) 3353–3358.
[9] X. Zhu, J. Hu, W. Wu, W. Zeng, H. Dai, Y. Du, Z. Liu, L. Li, H. Ji, Y. Zhu, J. Mater. Chem. A 2 (2014) 7812–7818.
[10] Y. Long, Y. Shu, X. Ma, M. Ye, Electrochim. Acta 117 (2014) 105–112.
[11] Y.H. Ding, H.M. Ren, Y.Y. Huang, F.H. Chang, P. Zhang, Mater. Res. Bull. 48 (2013) 3713–3716.
[12] S.D. Seo, I.S. Hwang, S.H. Lee, H.W. Shim, D.W. Kim, Ceram. Int. 38 (2012) 3017–3021.
[13] E.G. Bae, Y.H. Hwang, M. Pyo, Bull. Korean Chem. Soc. 34 (2013) 1199–1204.
[14] Z.S. Wu, S. Pei, W. Ren, D. Tang, L. Gao, B. Liu, F. Li, C. Liu, H.M. Cheng, Adv. Mater. 21 (2009) 1756–1760.
[15] K.V. Sreelakshmi, S. Sasi, A. Balakrishnan, N. Sivakumar, A.S. Nair, S.V. Nair, K.R.V. Subramanian, Energy Technol. 2 (2014) 257–262.
[16] W.S. Hummers, R.E. Offeman, J. Am. Chem. Soc. 80 (1958) 1339.
[17] K.N. Kudin, B. Ozbas, H.C. Schniepp, R.K. Prud'homme, I.A. Aksay, R. Car, Nano Lett. 8 (2008) 36–41.
[18] S. Stankovich, D.A. Dikin, R.D. Piner, K.A. Kohlhaas, A. Kleinhammes, Y. Jia, Y. Wu, S.T. Nguyen, R.S. Ruoff, Carbon 45 (2007) 1558–1565.
[19] Y. Ding, Y. Jiang, F. Xu, J. Yin, H. Ren, Q. Zhuo, Z. Long, P. Zhang, Electrochem. Commun. 12 (2010) 10–13.

[20] B. Gao, G.Z. Yue, Q. Qiu, Y. Cheng, H. Shimoda, L. Fleming, O. Zhou, Adv. Mater. 13 (2001) 1770–1773.
[21] X. Wang, L. Zhi, K. Müllen, Nano Lett. 8 (2007) 323–327.
[22] B. Wang, B. Xu, T. Liu, P. Liu, C. Guo, S. Wang, Q. Wang, Z. Xiong, D. Wang, X.S. Zhao, Nanoscale 6 (2014) 986–995.
[23] E. Barsoukov, J.R. Macdonald, Impedance Spectroscopy: Theory, Experiment, and Applications, second ed., Wiley, Hoboken, NJ, 2005.
[24] R. Ruffo, S.S. Hong, C.K. Chan, R.A. Huggins, Y. Cui, J. Phys. Chem. C 113 (2009) 11390–11398.